Eur. Phys. J. D **22**, 141–156 (2003)
DOI: 10.1140/epjd/e2002-00234-8

THE EUROPEAN PHYSICAL JOURNAL D

Evolution of cat states in a dissipative parametric amplifier: decoherence and entanglement

Faisal A.A. El-Orany[1], J. Peřina[2], V. Peřinová[2], and M. Sebawe Abdalla[3,a]

[1] Department of Mathematics and Computer Science, Faculty of Natural Science, Suez Canal University, Ismailia, Egypt
[2] Department of Optics[b], Palacký University, 17. listopadu 50, 772 07 Olomouc, Czech Republic
[3] Mathematics Department, College of Science, King Saud University, P.O. Box 2455, Riyadh 11451, Saudi Arabia

Received 25 September 2001 / Received in final form 30 May 2002
Published online 13 December 2002 –

Abstract. The evolution of the Schrödinger-cat states in a dissipative parametric amplifier is examined. The main tool in the analysis is the normally ordered characteristic function. Squeezing, photon-number distribution and reduced factorial moments are discussed for the single- and compound-mode cases. Also the single-mode Wigner function is demonstrated. In addition to the decoherence resulting from the interaction with the environment (damped case) there are two sources which can cause such decoherence in the system even if it is completely isolated: these are the decay of the pump and the relative phases of the initial cat states. Furthermore, for the damped case there are two regimes, which are underdamped and overdamped. In the first (second) regime the signal mode or the idler mode "collapses" to a statistical mixture (thermal field).

PACS. 42.50.Dv Nonclassical field states; squeezed, antibunched, and sub-Poissonian states; operational definitions of the phase of the field; phase measurements – 42.60.Gd Q-switching

1 Introduction

The linear superposition principle is at the heart of quantum mechanics since, using it, one can control the properties of the single states making them more or less pronounced. The most significant example reflecting the power of such a principle are the Schrödinger-cat states [1], which exhibit various nonclassical effects such as squeezing, sub-Poissonian statistics and oscillations in photon-number distribution [2–4], even if the original states are close to the classical ones [5]. Such type of states (of a jth mode for convenience) can be represented as

$$|\alpha\rangle_{\phi_j} = N_j[|\alpha_j\rangle + \exp(\mathrm{i}\phi_j)|-\alpha_j\rangle], \tag{1}$$

where $|\alpha_j\rangle$ is a coherent state of the jth mode with complex amplitudes α_j, ϕ_j is a relative phase and N_j is the normalization constant having the form

$$N_j^2 = \frac{1}{2[1+\exp(-2|\alpha_j|^2)\cos\phi_j]}\,. \tag{2}$$

Specifically there are three values of ϕ_j, namely, $0, \pi$ and $\pi/2$, for which (1) reduces to even coherent (ECS), odd coherent (OCS) and Yurke-Stoler (YSS) states, respectively. These three states will be frequently used in this paper.

There are several proposals for generating states (1) in various nonlinear processes, *e.g.* see [4,6–10]. Further, the evolution of cat states in several quantum systems has been intensively studied [11–18]. For convenience of the present work we refer to the interaction of these states with environment [11–14,18], where the common goal of such studies is the comprehension and description of the decoherence processes (decoherence is the rapid transformation of a pure linear superposition state into the corresponding statistical mixture state) in the system under observation, and the energy loss due to the interaction with the reservoir. Most of these papers adopt the Heisenberg–Langevin approach or the Markov master equation approach. Although the non-Markovian dynamics is important in quantum physics (theory), a unified and compact treatment of the non-Markovian reservoirs dates as late from [19], where also the decay and revival of the Schrödinger-cat states are characterized.

On the other hand, parametric amplifier (nondegenerate) takes a considerable interest in quantum optics since it can perfectly generate two-mode squeezing. Recently, this device has been supported with the fast progress of new nonlinear crystals and improved laser sources, especially femtosecond lasers [20] and it has been employed in

[a] e-mail: sebaweh@awalnet.net.sa
[b] Joint Laboratory of Optics of Palacký University and Institute of Physics, Academy of Sciences of the Czech Republic, 17. listopadu 50, 772 07 Olomouc, Czech Republic.

experiments, *e.g.* in the interference experiments [21,22]. An investigation of the statistical properties of the parametric amplifier with losses [23] and without losses [24–26] for compound-mode case have been performed using different techniques when the modes are initially prepared in the coherent states. The anticorrelation in this model is an interesting effect [26], where also under certain conditions the variance of the photon number is less than the average photon number and the photocounting distribution becomes narrower than the corresponding Poisson distribution for a coherent state with the same mean photon number. Moreover, the sum photon-number distribution can exhibit collapses and revivals [27] (and references therein) similar to those typical in the Jaynes-Cummings model (JCM) [28]; the former is in the photon number domain rather than the time domain. So the question we would like to address in this paper is the following: what would be the influence of the interference in phase space on these phenomena? In other words, we study the evolution of the cat states (1) through the parametric amplifier and take into account the interaction with environment. The system alone may be described by tracing a more complete description over the environment. Actually, the interaction considered here is quite different from that considered in [11–17] because there are two operations controlling its behaviour, which are the interference in phase space and the entanglement (correlation) between the signal and idler modes as well as between the signal-idler system and the environmental oscillators (reservoirs) to which the system may be connected. Such entanglements lead to the increase of the marginal entropies of the subsystems (as is known, if the density operator describes pure states, then the entropy (S) is zero, otherwise $S \neq 0$) [29]). For the present system we treat the single- and compound-mode cases. The main tools in our treatment are the normally ordered characteristic functions. The Hamiltonian which governs the interaction is [30,31]

$$\hat{H} = \hbar \sum_{j=1}^{2} \omega_j \hat{a}_j^{\dagger} \hat{a}_j - \hbar g [\hat{a}_1 \hat{a}_2 \exp(\mathrm{i}\omega t - \mathrm{i}\phi) + \mathrm{h.c.}] + \hbar \sum_{j=1}^{2} \sum_{l=1}^{\infty} \left[\varphi_{jl} \hat{b}_{jl}^{\dagger} \hat{b}_{jl} + k_{jl} \hat{b}_{jl} \hat{a}_j^{\dagger} + k_{jl}^{*} \hat{b}_{jl}^{\dagger} \hat{a}_j \right], \quad (3)$$

where $\hat{a}_j$, $(\hat{a}_j^{\dagger})$, $j = 1, 2$, are the annihilation (creation) operators assigned to the signal and idler modes, respectively; ω_j are the natural frequencies of oscillations of the uncoupled modes with $\omega = \omega_1 + \omega_2, \omega$ being a pump frequency (under the assumption of resonance frequency); ϕ is the initial phase of the pump and h.c. means the Hermitian conjugate term to the previous one; g is the real coupling constant including the amplitude of the pump (gain coefficient); $\hat{b}_{jl}$ and $\hat{b}_{jl}^{\dagger}$ are the boson annihilation and creation operators of the reservoir oscillators, respectively, with the frequencies φ_{jl}, and k_{jl} are the coupling constants of the system-reservoirs interaction. Hamiltonian (3) represents three wave mixing in a nonlinear crystal described by the second-order susceptibility $\chi^{(2)}$. Specifically, a pump beam with frequency ω travelling through the crystal creates photons of the signal and idler modes with different frequencies ω_j, $j = 1, 2$, such that $\omega = \omega_1 + \omega_2$. The whole system is considered to be interacting with its surroundings (*e.g.*, *via* imperfect cavity mirrors), which are modelled as reservoirs.

For completeness, the well-known solution of the Heisenberg–Langevin equations for the Hamiltonian (3) is [30,31]

$$\begin{aligned} \hat{A}_1(t) &= f_1(t)\hat{a}_1(0) + f_2(t)\hat{a}_2^{\dagger}(0) + \sum_{l}^{\infty} \left[\hat{b}_{1l}(0) \Gamma_{1l}(t) + \hat{b}_{2l}^{\dagger}(0) \Gamma'_{1l}(t) \right], \\ \hat{A}_2(t) &= f_3(t)\hat{a}_2(0) + f_2(t)\hat{a}_1^{\dagger}(0) + \sum_{l}^{\infty} \left[\hat{b}_{1l}^{\dagger}(0) \Gamma_{2l}(t) + \hat{b}_{2l}(0) \Gamma'_{2l}(t) \right], \end{aligned} \quad (4)$$

where $\hat{A}_j(t) = \hat{a}_j(t) \exp(\mathrm{i}\omega_j t)$; $\hat{a}_j(0)$ and $\hat{b}_{jl}(0)$, $j = 1, 2$, are the initial operators of the modes and reservoirs, respectively. The explicit forms for the dynamical coefficients $f_j(t), \Gamma_{jl}(t)$ and $\Gamma'_{jl}(t)$ are given in Appendix A. Further, it is worth mentioning that the Langevin forces have the forms

$$\hat{L}_j(t) = -\mathrm{i} \sum_{l} k_{jl} \hat{b}_{jl}(0) \exp(-\mathrm{i}\varphi_{jl} t), \quad j = 1, 2. \quad (5)$$

These forces satisfy the following commutation rule

$$[\hat{L}_j(t), \hat{L}_{j'}^{\dagger}(t')] = \gamma_j \delta_{jj'} \delta(t - t') \hat{1}, \quad (6)$$

where γ_j is the cavity decay rate of the jth mode (for more details about the properties of the reservoir oscillators, see [25,32]). Finally it is worth mentioning that including lossy mechanism, the difference mean-photon number between the signal and idler modes in the system becomes nonconservative.

This paper is organized as follows: in Section 2 the basic equations and relations, such as two-mode normally ordered characteristic function, quadrature squeezing, Wigner function, reduced factorial moments and photon-number distribution are given when the modes are initially prepared in the cat states (1). In Sections 3 and 4 discussion of the results of the single-mode and compound-mode cases are performed, respectively, and the conclusions are summarized in Section 5.

2 Basic relations and equations

In this section we give the main relations which will be used to investigate the properties of the system under consideration. Actually, the calculations are lengthy, but straightforward, and for this reason, we give briefly general calculations in such a way that particular results can be obtained using suitable choice of parameters. We start by discussing the initial density matrix of the system. We assume that the system and reservoirs are initially independent and noninteracting before switching on the interaction, and the interaction between them starts at $t = 0$.

This means that the density operator could be written initially as a direct product [33]:

$$\hat{\rho}(0) = \hat{\rho}_{\rm f}(0) \otimes \hat{\rho}_{\rm r}(0), \tag{7}$$

where $\hat{\rho}_{\rm r}(0)$ is the density matrix of the system of damping oscillators, which we assume to have flat (*i.e.* constant function of frequency) and broad-band reservoir spectra, so that the mean number of reservoir quanta (phonons) in the mode l is $\langle \hat{b}^{\dagger}_{jl}(0)\hat{b}_{jl}(0)\rangle = \langle \hat{n}_{jd}\rangle$ independently of l, where the subscript d denotes broad-band reservoir. Also we assume that the reservoirs form chaotic systems with mean photon numbers $\langle \hat{n}_{jd}\rangle = [\exp(\hbar\varphi_j/TK_{\rm B}) - 1]^{-1}$, where the reservoirs-oscillators are at the temperature T, with the frequency φ_j, $K_{\rm B}$ is Boltzmann's constant and $\hbar$ Planck's constant divided by 2π. We proceed assuming that $\hat{\rho}_{\rm f}(0)$ is the field density operator, which in our case, where the modes are assumed to be initially in superposition states (1), has the form

$$\begin{aligned}\hat{\rho}_{\rm f}(0) &= |\alpha\rangle_{\phi_1}|\alpha\rangle_{\phi_2\phi_2}\langle\alpha|_{\phi_1}\langle\alpha| \\ &= N_1^2 N_2^2 \sum_{j',j=1}^{4} \exp({\rm i}\phi_{j'} + {\rm i}\phi'_j)|\alpha_{j'}\rangle|\alpha_j\rangle\langle\alpha'_j|\langle\alpha'_{j'}| \\ &= N_1^2 N_2^2[\hat{\rho}_{\rm M}(0) + \hat{\rho}_{\rm SI}(0) + \hat{\rho}_{\rm AI}(0)]. \end{aligned} \tag{8}$$

The concise form in the second line of (8) means that the values of $\alpha_j, \phi_j, \alpha'_j$ and ϕ'_j should be specified to obtain the exact form of the density operator in the first line. Here $\hat{\rho}_{\rm M}(0)$ denotes the statistical mixture part of the density operator as

$$\begin{aligned}\hat{\rho}_{\rm M}(0) = {} & |\alpha_1\rangle|\alpha_2\rangle\langle\alpha_2|\langle\alpha_1| + |\alpha_1\rangle| - \alpha_2\rangle\langle-\alpha_2|\langle\alpha_1| \\ & + |-\alpha_1\rangle|\alpha_2\rangle\langle\alpha_2|\langle-\alpha_1| + |-\alpha_1\rangle| - \alpha_2\rangle\langle-\alpha_2|\langle-\alpha_1|; \end{aligned} \tag{9}$$

$\hat{\rho}_{\rm SI}(0)$ denotes symmetric interference part of the density operator in which the two modes are in off-diagonal basis of coherent states and can be written as

$$\begin{aligned}\hat{\rho}_{\rm SI}(0) = {} & \Big\{\exp[{\rm i}(\phi_1+\phi_2)]|-\alpha_1\rangle| - \alpha_2\rangle\langle\alpha_2|\langle\alpha_1| \\ & + \exp[-{\rm i}(\phi_1+\phi_2)]|\alpha_1\rangle|\alpha_2\rangle\langle-\alpha_2|\langle-\alpha_1|\Big\} + {\rm h.c.} \end{aligned} \tag{10}$$

and $\hat{\rho}_{\rm AI}(0)$ denotes asymmetric interference part of the density operator in which one of the modes is in a diagonal coherent states basis while the other is in off-diagonal basis or *vice versa* and reads:

$$\begin{aligned}\hat{\rho}_{\rm AI}(0) = {} & \Big\{\exp(-{\rm i}\phi_1)\Big[|\alpha_1\rangle|\alpha_2\rangle\langle\alpha_2|\langle-\alpha_1| \\ & + |\alpha_1\rangle| - \alpha_2\rangle\langle-\alpha_2|\langle-\alpha_1|\Big] \\ & + \exp(-{\rm i}\phi_2)\Big[|\alpha_1\rangle|\alpha_2\rangle\langle-\alpha_2|\langle\alpha_1| \\ & + |-\alpha_1\rangle|\alpha_2\rangle\langle-\alpha_2|\langle-\alpha_1|\Big]\Big\} + {\rm h.c.} \end{aligned} \tag{11}$$

The quantum properties of the system can be traced *via* the evolution of the normally ordered characteristic function, which for the two-mode case has the form

$$C_{\mathcal{N}}(\zeta_1,\zeta_2,t) = {\rm Tr}\left\{\hat{\rho}(0)\prod_{j=1}^{2}\exp[\zeta_j\hat{A}_j^{\dagger}(t)]\exp[-\zeta_j^{*}\hat{A}_j(t)]\right\}, \tag{12}$$

where, for the system under consideration, $\hat{A}_j(t)$ are given in (4) and $\hat{\rho}(0)$ is the initial density operator of the system (7). It is obvious that the characteristic function here includes 16 elements [34]. We give only the calculations related to the element $\exp({\rm i}\phi_1 + {\rm i}\phi'_2)|\alpha_1\rangle|\alpha_2\rangle\langle\alpha'_2|\langle\alpha'_1|$ of the density matrix. On substituting this element together with (4) into (12) and calculating the expectation values, we arrive at

$$\begin{aligned} I(\zeta_1,\zeta_2,t) = {} & \exp\left[{\rm i}\phi_1 + {\rm i}\phi'_2 - \frac{1}{2}\sum_{j=1}^{2}(|\alpha_j|^2 + |\alpha'_j|^2 - 2\alpha_j^{*}\alpha'_j)\right] \\ & \times \exp\Bigg\{\zeta_1\zeta_2 D(t) + \zeta_1^{*}\zeta_2^{*}D^{*}(t) \\ & - \left[\sum_{j=1}^{2}|\zeta_j|^2 B_{j\mathcal{N}}(t)\right] + \sum_{j=1}^{2}[\zeta_j\bar{\alpha}_j(t) - \zeta_j^{*}\bar{\alpha}'_j(t)]\Bigg\}, \end{aligned} \tag{13}$$

the explicit forms of the quantities $B_{j\mathcal{N}}(t), D(t), D^{*}(t)$ and $\bar{\alpha}_j(t)$ are given in Appendix B. It is worth mentioning that throughout the calculation of (13), the standard commutator of the Langevin forces (6) and the usual Wigner-Weisskopf approximation have been used, which leads to a replacement of the coupling constants by the cavity decay rates $\gamma_j \geq 0$. More details about the calculation of (13) can be found in [30,31]. On the other hand, the characteristic function of the single-mode case can be obtained from that of the two-mode case by simply setting the parameter related to the absent mode equal to zero, *e.g.* the characteristic function of the signal mode (first-mode) can be obtained by setting $\zeta_2 = 0$ in (12) and (13).

The different moments of the bosonic operator system can be determined by differentiation of the normally ordered characteristic function through the relation

$$\left\langle\prod_{j=1}^{2}\hat{A}_j^{\dagger m_j}(t)\hat{A}_j^{n_j}(t)\right\rangle = \prod_{j=1}^{2}\frac{\partial^{m_j+n_j}}{\partial\zeta_j^{m_j}\partial(-\zeta_j^{*})^{n_j}}C_{\mathcal{N}}(\zeta_1,\zeta_2,t)|_{\zeta_1=\zeta_2=0}. \tag{14}$$

In order to investigate squeezing property for the compound-mode case we can define the two quadrature operators $\hat{X}(t) = (1/2)\sum_{j=1}^{2}[\hat{A}_j(t) + \hat{A}_j^{\dagger}(t)]$, $\hat{Y}(t) = (1/2{\rm i})\sum_{j=1}^{2}[\hat{A}_j(t) - \hat{A}_j^{\dagger}(t)]$, where

$[\hat{X}(t), \hat{Y}(t)] = \mathrm{i}\hat{1}$ and then the uncertainty relation reads $\langle(\Delta\hat{X}(t))^2\rangle\langle(\Delta\hat{Y}(t))^2\rangle \geq 1/4$, where, *e.g.* $\langle(\Delta\hat{X}(t))^2\rangle = \langle(\hat{X}(t))^2\rangle - \langle\hat{X}(t)\rangle^2$. Therefore, we can say that the system is able to yield two-mode squeezing if the squeezing factor $S(t) = 2\langle(\Delta\hat{X}(t))^2\rangle - 1 < 0$ or $Q(t) = 2\langle(\Delta\hat{Y}(t))^2\rangle - 1 < 0$. Similar quantities can be defined for the single-mode case.

We proceed to the two-mode normal generating function which is defined as

$$C_{\mathcal{N}}^{(W)}(\lambda,t) = \frac{1}{(\pi\lambda)^2}\iint \exp\left(-\frac{1}{\lambda}\sum_{j=1}^{2}|\zeta_j|^2\right) \times C_{\mathcal{N}}(\zeta_1,\zeta_2,t)\mathrm{d}^2\zeta_1\mathrm{d}^2\zeta_2. \quad (15)$$

This function may be used in studying the sum photon-number distribution and the reduced factorial moments for compound modes. For the general term (13), relation (15) can be calculated to obtain

$$I_{\mathcal{N}}^{(W)}(\lambda,t) = \frac{1}{(1+\lambda\lambda_+)(1+\lambda\lambda_-)}\exp\left[\frac{A_+\lambda}{1+\lambda\lambda_+}+\frac{A_-\lambda}{1+\lambda\lambda_-}\right] \times \exp\left[\mathrm{i}\phi_1+\mathrm{i}\phi_2'-\frac{1}{2}\sum_{j=1}^{2}(|\alpha_j|^2+|\alpha_j'|^2-2\alpha_j^*\alpha_j')\right], \quad (16)$$

where

$$\lambda_\pm = \frac{1}{2}[B_{1\mathcal{N}}(t)+B_{2\mathcal{N}}(t)] \pm \frac{1}{2}\sqrt{[B_{1\mathcal{N}}(t)-B_{2\mathcal{N}}(t)]^2+4|D(t)|^2},$$
$$A_\pm = \frac{\pm 1}{\lambda_- - \lambda_+}\Big\{\bar{\alpha}_1'(t)\bar{\alpha}_2'(t)D(t)+\bar{\alpha}_1(t)\bar{\alpha}_2(t)D^*(t) - \bar{\alpha}_1(t)\bar{\alpha}_1'(t)[B_{2\mathcal{N}}(t)-\lambda_\pm] - \bar{\alpha}_2(t)\bar{\alpha}_2'(t)[B_{1\mathcal{N}}(t)-\lambda_\pm]\Big\}. \quad (17)$$

Expression (16) shows that each term of the generating function of the system is the two-fold generating function for Laguerre polynomials. Further, in each term the quantities $A_\pm$ and $\lambda_\pm$ play the role of the mean numbers of coherent photons and mean numbers of chaotic photons, respectively. The sum photon-number distribution $P(n,t)$ and the reduced factorial moments $\langle W^k(t)\rangle$ for the compound-mode case can be defined by means of the derivative of $C_{\mathcal{N}}^{(W)}(\lambda,t)$ *via* the relations

$$P(n,t) = \frac{(-1)^n}{n!}\frac{\mathrm{d}^n}{\mathrm{d}\lambda^n}C_{\mathcal{N}}^{(W)}(\lambda,t)\Big|_{\lambda=1},$$
$$\langle W^k(t)\rangle = (-1)^k\frac{\mathrm{d}^k}{\mathrm{d}\lambda^k}C_{\mathcal{N}}^{(W)}(\lambda,t)\Big|_{\lambda=0}. \quad (18)$$

On using (16), these quantities can be deduced to become

$$P_I(n,t) = \frac{1}{(1+\lambda_-)(1+\lambda_+)}\exp\left[\frac{A_-}{1+\lambda_-}+\frac{A_+}{1+\lambda_+}\right] \times \exp\left[\mathrm{i}\phi_1+\mathrm{i}\phi_2'-\frac{1}{2}\sum_{j=1}^{2}(|\alpha_j|^2+|\alpha_j'|^2-2\alpha_j^*\alpha_j')\right] \times \sum_{l=0}^{n}\frac{1}{(n-l)!l!}\left(\frac{\lambda_-}{1+\lambda_-}\right)^{n-l}\left(\frac{\lambda_+}{1+\lambda_+}\right)^{l} \times L_{n-l}[\frac{A_-}{\lambda_-(1+\lambda_-)}]L_l\left[\frac{A_+}{\lambda_+(1+\lambda_+)}\right], \quad (19)$$

$$\langle W_I^k(t)\rangle = \exp\left[\mathrm{i}\phi_1+\mathrm{i}\phi_2'-\frac{1}{2}\sum_{j=1}^{2}(|\alpha_j|^2+|\alpha_j'|^2-2\alpha_j^*\alpha_j')\right] \times \sum_{l=0}^{k}\binom{k}{l}\lambda_-^{k-l}\lambda_+^l L_{k-l}\left(\frac{A_-}{\lambda_-}\right)L_l\left(\frac{A_+}{\lambda_+}\right), \quad (20)$$

where the subscript I in (19) and (20) means that these quantities have been calculated for the general term (13). Also in (19) and (20) $L_n(.)$ are the Laguerre polynomials of order n having the form

$$L_n(x) = \sum_{m=0}^{n}\frac{(n!)^2(-x)^m}{(n-m)!(m!)^2}\cdot \quad (21)$$

We should mention that the phase terms, *e.g.* the term in the second line of (19), exist only in the off-diagonal elements indicating that these elements are suppressed faster than the diagonal elements. In other words, the greater the "distance" between the components of the cat states, the more rapidly the off-diagonal elements are damped.

On the other hand, the corresponding quantities for the single-mode case can be obtained with the help of the single-mode normally ordered characteristic function and applying the same procedures as before. To be more specific, a general term $I'(\zeta_1,t)$ of the first-mode case can be obtained from (13) by setting $\zeta_2 = 0$ and consequently the corresponding photon-number distribution and the reduced factorial moments are

$$P_{I'}(n_1,t) = \exp\left[\mathrm{i}\phi_1+\mathrm{i}\phi_2'-\frac{\bar{\alpha}_1(t)\bar{\alpha}_1'(t)}{1+B_{1\mathcal{N}}(t)} -\frac{1}{2}\sum_{j=1}^{2}(|\alpha_j|^2+|\alpha_j'|^2-2\alpha_j^*\alpha_j')\right] \times \left[\frac{B_{1\mathcal{N}}(t)}{1+B_{1\mathcal{N}}(t)}\right]^{n_1}\frac{1}{1+B_{1\mathcal{N}}(t)} \times L_{n_1}\left[\frac{-\bar{\alpha}_1(t)\bar{\alpha}_1'(t)}{B_{1\mathcal{N}}(t)(1+B_{1\mathcal{N}}(t))}\right], \quad (22)$$

$$\langle W^k_{I'}(t)\rangle = \exp\left[\mathrm{i}\phi_1 + \mathrm{i}\phi'_2 - \frac{1}{2}\sum_{j=1}^{2}(|\alpha_j|^2 + |\alpha'_j|^2 - 2\alpha^*_j\alpha'_j)\right] \times B^k_{1\mathcal{N}}(t) L_k\left[\frac{-\bar{\alpha}_1(t)\bar{\alpha}'_1(t)}{B_{1\mathcal{N}}(t)}\right]. \quad (23)$$

Finally, the quantum properties of the system can be visualized well by analyzing its Wigner function (W). Actually, this function is sensitive to the interference in phase space and therefore it is helpful to be examined. The single-mode Wigner function is defined as

$$W(z,t) = \pi^{-2}\int \mathrm{d}^2\zeta_1 \exp\left(-\frac{1}{2}|\zeta_1|^2\right) \times C_{\mathcal{N}}(\zeta_1,t)\exp(z\zeta^*_1 - \zeta_1 z^*), \quad (24)$$

where $C_{\mathcal{N}}(\zeta_1,t)$ is the single-mode normally ordered characteristic function. The Wigner function for the single-mode general term is

$$W_{I'}(z,t) = \frac{2}{\pi[1+2B_{1\mathcal{N}}(t)]}\exp\Big[\mathrm{i}\phi_1 + \mathrm{i}\phi'_2 - \frac{1}{2}\sum_{j=1}^{2}\big(|\alpha_j|^2 + |\alpha'_j|^2 - 2\alpha^*_j\alpha'_j\big)\Big] \times \exp\left\{-2\frac{[\bar{\alpha}^*_1(t) - z^*][\bar{\alpha}'_1(t) - z]}{1+2B_{1\mathcal{N}}(t)}\right\}. \quad (25)$$

In this expression $B_{1\mathcal{N}}(t)$ is always positive and represents the sum of quantum noises in the field, related to quantum fluctuations in the interaction and the mean value of reservoirs oscillators (the number of photons or phonons transferred from the reservoirs to the quantum system). This shows that the width of this part of W function becomes broader when the coupling with environment is considered.

In the following sections we analyze the behaviour of the system under discussion on the basis of the results of the present section. We investigate the properties of both the single-mode and compound-mode cases.

3 Results for the single-mode case

In our analysis for the dissipative case we consider symmetrical losses that is $\gamma_j = \gamma$ and $\langle \hat{n}_{jd}\rangle = \bar{n}$ for $j = 1, 2$. We analyze two cases: underdamped case when $2g > \gamma$ and overdamped case when $2g < \gamma$. The origin of these conditions can easily be recognized by careful examination of the time dependent coefficients in Appendix A. For example, it holds that

$$f_1(t) = \frac{1}{2}\left\{\exp\left[\left(g - \frac{\gamma}{2}\right)t\right] + \exp[-(g+\frac{\gamma}{2})t]\right\}. \quad (26)$$

In the following we discuss the behaviour of W function, photon-number distribution, squeezing and reduced factorial moments for the single-mode case.

3.1 Wigner function

Investigation of the single-mode W function is important since it is informative and sensitive to the interference in phase space, and also it gives a prediction to the possible occurrence of the nonclassical effects in the system. Furthermore, this function can be obtained experimentally using the optical homodyne tomography [35].

In general, the W functions of ECS, OCS and YSS (at $t = 0$) are consisting of two Gaussian bells, resulting from statistical mixture of individual composite states and interference fringes in between (signature of the nonclassical effects) originating from the superposition between different components of the states. Nevertheless, the locations of the extreme values of the interference fringes of ECS, OCS and YCS are quite different. There are several papers, *e.g.*, [11,12,18,36] that have been devoted to these fringes making them less or more pronounced by allowing the cat states to evolve in different quantum optical systems. For example, the decay rate of the interference fringes of the W function of cat states of a mode which is coupled to a phase-sensitive reservoir (squeezed reservoirs) [12], (also [34] p. 114), can be smaller or larger than that for ordinary thermal heat bath reservoir [11]. Furthermore, in these systems the fringes can be washed out completely for a specific choice of the interaction parameters. In the language of the density matrix this means that the contribution of the off-diagonal elements is small compared with the contribution of the diagonal elements but it is not necessarily zero. Of course, such diagonalization produces a statistical mixture of coherent states, which are close to classical wavepackets. Now if we consider the W function of the signal mode for the system under discussion, the situation becomes more complicated than before [11,12,18] owing to the entanglement between the signal and idler modes. The structure of the density matrix (8) carries more information, *e.g.*, when the signal and idler modes are initially prepared in a distinguishable macroscopic cat state and after switching on the interaction, the initial two Gaussian bells of the W function of the signal mode can be transformed, in principle, into fourfold form as indicated in (9), and the initial interference fringes of the cat will be dramatically changed during the interaction as a result of the competition between the different components of $\hat{\rho}_{\mathrm{AI}}(0)$ and $\hat{\rho}_{\mathrm{SI}}(0)$. Moreover, during evolution, the rate of movement of the centres of peaks of the W function is rather different and this leads to irregularity in its behaviour. So that the evolution of the cat states in the present interaction yields different types of multicomponent cat states [37]. All these facts can be seen in Figures 1a–1c, where we have displayed the W function for the signal mode (excluding losses) for the given values of the parameters. In these figures (and throughout this paper) we have taken $\alpha_j = |\alpha_j|\exp(\mathrm{i}\psi_j)$, where ψ_j is the phase of the initial amplitude of the jth mode and also we have defined z in (24) as $z = x + \mathrm{i}y$ where the quadrature variances $\langle(\Delta\hat{X}(t))^2\rangle$ and $\langle(\Delta\hat{Y}(t))^2\rangle$ of the signal mode are associated with the real part x and imaginary part y, respectively. It is worth mentioning that the W function curves contain most of their information within

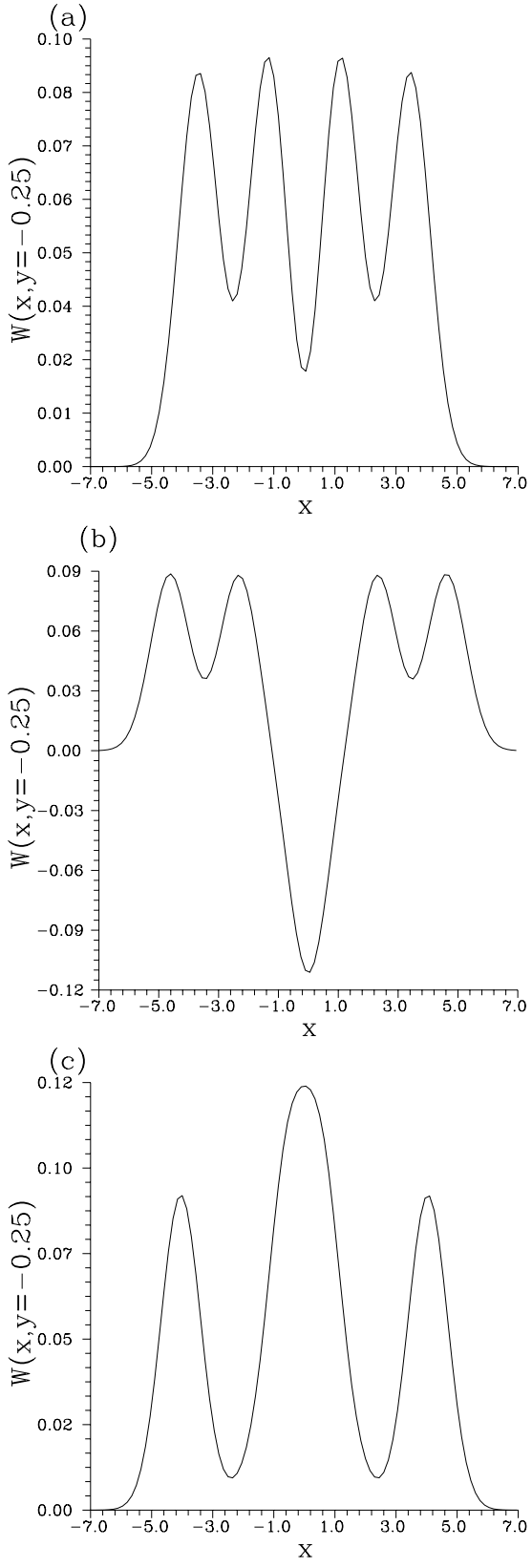

Fig. 1. The W function of the signal mode when the two modes (signal and idler) are initially in ECS for $t = 0.55, g = 1, \psi_1 = \psi_2 = 0, \gamma = \bar{n} = 0$ and $\phi = \pi/2$ and for: (a) $(|\alpha_1|, |\alpha_2|) = (2, 2)$; (b) $(|\alpha_1|, |\alpha_2|) = (3, 2)$; (c) $(|\alpha_1|, |\alpha_2|) = (2, 3)$.

one plane, in particular, for constant values of y. For this reason and for simplicity we have plotted a W function in one plane considering $y \simeq -0.25$, where the W function illustrates more pronounced nonclassical effects (*e.g.*, by means of negative values) for the case $|\alpha_1| > |\alpha_2|$ and also it includes a representative information for the other cases. Figure 1a shows that the initial nonclassical negative values of the W function have been smeared out and the system collapses to four-component statistical mixture state. Further, such behaviour reveals that decoherence can be established *via* the entanglement between different modes in the parametric processes. In these cases the single-mode behaviour undergoes amplification resulting from the spontaneous pump photon decay [38]. It should be borne in mind that in the present case the system is completely isolated and then such type of decoherence can be called nondissipative decoherence [39]. On the other hand, the nonclassical negative values can be recovered by controlling the "distance" between the initial cat states of the signal and idler modes. To be more specific, when $|\alpha_1| > |\alpha_2|$ these negative values can be realized, however, when $|\alpha_2| > |\alpha_1|$ they will disappear as indicated in Figures 1b and 1c, respectively. In Figure 1c a three-peak structure is dominant. Comparison of Figures 1a, 1b and 1c is instructive. So, excluding the influence of the environment the system can decohere and recohere by adjusting the initial distance between the components of the cat of the input modes. However, for the dissipative case the decoherence process is related not only to the amplification of the pumping field but also to damping of radiation caused by the flux of coherent energy from radiation to the reservoirs and noise from reservoirs to the radiation. Under these circumstances the decoherence can be achieved in a time shorter than that for the undamped case. We displayed the W function for the overdamped and underdamped cases in Figures 2a and 2b, respectively, for the same situation as in Figure 1b. These figures show overall distortion due to the dissipative nature of dynamics. It is clear that the origin of the main contribution is in the diagonal elements of the density matrix and then the negative values of the W function of the undamped case (Fig. 1b) are washed out. From Figure 2a one can observe that the W function exhibits the well-known shape for the thermal light, *i.e.* the system exhibits Bose-Einstein statistics (super-classical light). However, from Figure 2b (underdamped case) we can observe that the two-peak structure is dominant. This situation is similar to that of the single harmonic oscillator interacting with the thermal bath in which a double Gaussian structure with missing oscillatory behaviour occurs [11,12,36]. The explanation of the behaviour of W function in Figure 2 can be understood by analyzing the behaviour of the W function for the single-mode general term (25). Let us restrict ourselves to the overdamped case for which the values of the parameters $\bar{\alpha}_j(t)$ are exponentially decaying (this can be easily checked) when the interaction is going on and accordingly the centres of the peaks move toward the origin and eventually the peaks merge with each other. The opposite situation occurs for the underdamped case. It is

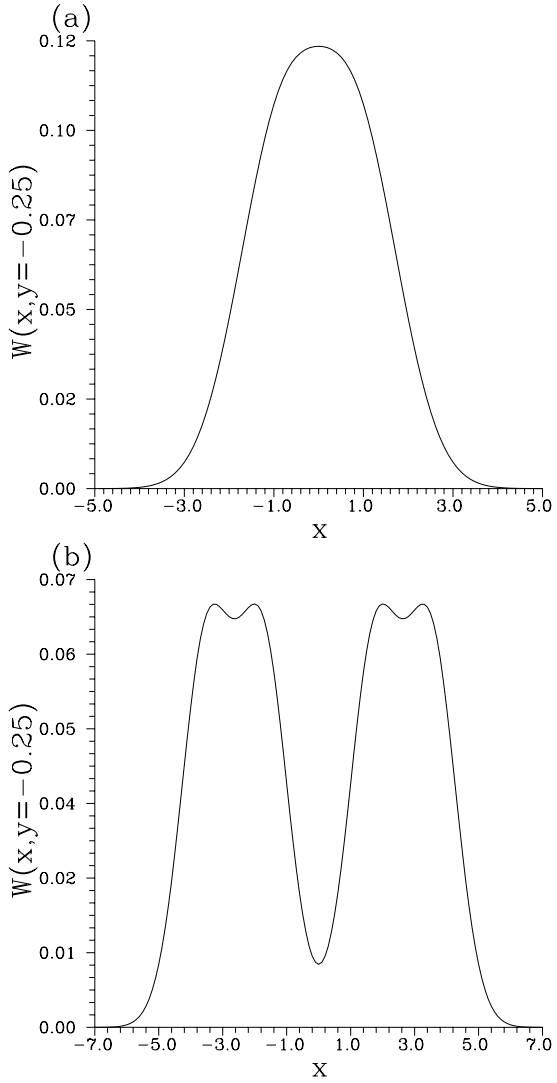

Fig. 2. The W function of the signal mode for the same situation as in Figure 1b except $\bar{n} = 1$ and (a) overdamped case $\gamma = 2g + 3$; (b) underdamped case $\gamma = 2g - 1$.

worth mentioning that in these cases (overdamped and underdamped cases) the contribution of the off-diagonal elements corresponding to $\hat{\rho}_{\rm AI}(0)$ is suppressed faster than that of $\hat{\rho}_{\rm SI}(0)$. This point will be discussed in the sum photon-number distribution in the following section.

In general, if the interaction between different components in the system occurs (regardless whether the interaction with environment is considered or not), the decoherence gradually increases and thus the system evolves into a mixture ($\mathrm{Tr}\hat{\rho}_1^2(t) < 1$, $\hat{\rho}_1(t)$ is the reduced density matrix of the signal mode), *i.e.* there occurs a destruction of the inherent nonclassical effects. The rate of destruction is sensitive to the nature of both the reservoir and parametric processes. Furthermore, we should mention that the P function possesses somewhat similar behaviour as the W function in such a case, *i.e.* it can take on negative values in certain regions for certain values of the parameters and therefore it cannot behave like a classical probability distribution function. Such an effect is independent of the type of cat states, which are initially used in the interaction. Finally, we should stress that it is difficult to analyze the behaviour of the off-diagonal elements to obtain concrete information, so we have basically concentrated on the computer simulation.

3.2 Photon-number distribution

The concept of photon is an integral part of the modern description of light and the discrete nature of light can be demonstrated by a photon detector based on the photoelectric effect.

On the other hand, one of most interesting nonclassical effects emerging from the superposition principle is the oscillatory behaviour of the photon-number distribution. In general, such behaviour is closely related to the behaviour of the W function, however, this is necessary but not sufficient condition. For example, the photon-number distributions of ECS, OCS and YSS are completely different; whereas those of ECS and OCS exhibit pairwise oscillations in phase space (even number of photons can be observed for ECS and odd numbers for OCS), the distribution of YSS is a Poissonian even though the behaviour of the W function for these states is qualitatively similar. In the interaction under discussion for undamped case the oscillatory behaviour in the photon-number distribution can be established even if the initial cat states exhibit Poissonian statistics. This is of course based on the values of the interaction parameters. The origin of such behaviour is in the interference in phase space where the photon-number distribution of input coherent light is always displaying a single-peak structure, which is broader than the corresponding Poisson distribution with the same mean photon number.

We start our discussion by investigating the behaviour of the undamped case. We consider here the photon-number distribution $P(n_1)$ of the signal mode when the signal and idler modes are initially prepared in the YSS. We have seen that this quantity can exhibit oscillatory behaviour after switching on of the interaction by a suitable time provided that $|\alpha_1| > |\alpha_2|$, as indicated in Figure 3 for shown values of the parameters. In this figure $\psi = \phi - \psi_1 - \psi_2$, where ψ_j is the phase of the initial jth mode (signal or idler) and ϕ is the phase of the pump as before. In this case ψ represents the phase mismatch. Furthermore, one can see that when ψ changes from $\pi/2$ to $-\pi/2$ the parity of oscillations changes (compare dashed and solid curves). The reason for taking $\psi = \pm\pi/2$ can be found in [27]. The origin of the oscillatory behaviour in the photon-number distribution $P(n_1)$ here is the competition between the contributions of $\hat{\rho}_{\rm M}(0)$ and of $\hat{\rho}_{\rm SI}(0)$, as we will see in the sum photon-number distribution. Further, it is worth mentioning that the behaviour of $P(n_1)$ in Figure 3 is similar to that of initially cat state of a mode coupled to a phase-sensitive reservoir [12], (also [34] p. 114), however, the source of the oscillations in [12] is the phase information included in the reservoir, which can be transferred to the field. In Figure 4

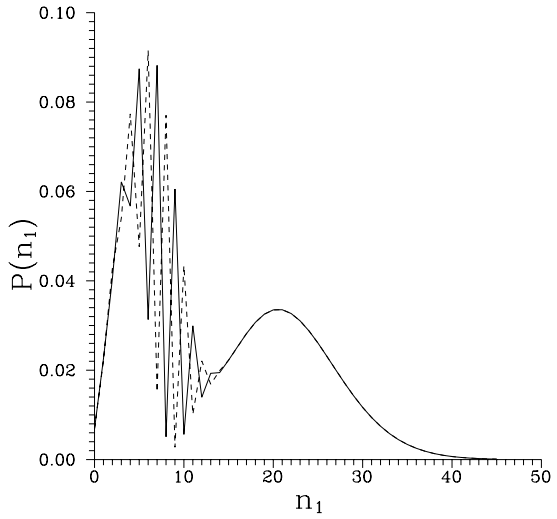

Fig. 3. Single-mode photon-number distribution of the signal mode when the signal and idler modes are prepared initially in YSS; the values of the parameters are the same as in Figure 1b and $\psi = \pi/2$ (solid curve), $-\pi/2$ (dashed curve).

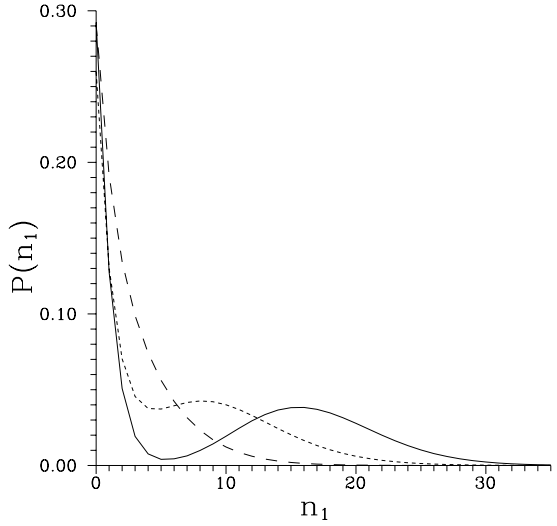

Fig. 4. Single-mode photon-number distribution of the signal mode when the signal and idler modes are prepared initially in YSS, the values of the parameters are the same as in Figure 1c with $\psi = \pi/2$ for $\gamma = \bar{n} = 0$ (undamped case-solid curve); $\bar{n} = 1, \gamma = 2g - 1$ (underdamped case-short-dashed curve); $\bar{n} = 1, \gamma = 2g + 1$ (overdamped case-long-dashed curve).

we have displayed $P(n_1)$ for the same situation as given by the solid curve in Figure 3, but for $|\alpha_1| < |\alpha_2|$ (solid curve); further the damped cases are considered: underdamped case (short-dashed curve) and overdamped case (long-dashed curve). Comparing the solid curves in Figures 3 and 4, we see from Figure 4 that the oscillations in $P(n_1)$ are smoothed out. Further, the comparison of various curves in Figure 4 shows that the behaviour of $P(n_1)$ for underdamped and undamped cases is similar in the sense that they include smooth oscillations. These smooth oscillations are completely washed out for the overdamped case, as is expected. Actually, for $|\alpha_2| > |\alpha_1|$ coherence is lost and the main contribution is related to the energy of the field mode (diagonal terms). As we can see the behaviour of the photon-number distribution is in a good agreement with that of W function. Finally, it has been verified that the behaviour of $P(n_1)$ for the damped case when $|\alpha_1| > |\alpha_2|$ and $|\alpha_1| < |\alpha_2|$ is quite similar. This is connected with the fact that the oscillatory behaviour in the photon-number distribution is highly sensitive to the dissipation dynamics.

3.3 Single-mode squeezing and reduced factorial moments

Squeezing is one of the most important phenomena in quantum optics because of its applications in various areas, *e.g.* in optics communication, quantum information theory, etc. [40]. Squeezed light can be measured by a homodyne detection in which the signal is superimposed on a strong coherent beam of the local oscillator. Furthermore, quite recently it has been shown experimentally that there is an evidence of squeezed light in the biological systems [41]. So an analysis of squeezing phenomenon in quantum optical systems is an important topic.

We start our investigation by determining the behaviour of the single-mode squeezing. Generally, in the system under consideration the output mode loses its initial squeezing feature during the interaction [16] as a result of an amplification process and the interaction with the environment, which accelerates the loss in quantum fluctuations. Here we analyze the influence of different types of cat states on the behaviour of quadrature squeezing. To do so, considering α_j to be real, we write down the quadrature variance of the Y-component (which is expected to yield squeezing) for the signal mode and various initial input cat states as follows:

$$Q_{\rm ee}(t) = \frac{1}{2}\Big\{B_{1\mathcal{N}}(t) + \alpha_1^2 f_1^2(t)(\tanh\alpha_1^2 - 1) + \alpha_2^2|f_2(t)|^2[\tanh\alpha_2^2 + \cos(2\phi)]\Big\}, \tag{27}$$

$$Q_{\rm oe}(t) = \frac{1}{2}\Big\{B_{1\mathcal{N}}(t) + \alpha_1^2 f_1^2(t)(\coth\alpha_1^2 - 1) + \alpha_2^2|f_2(t)|^2[\tanh\alpha_2^2 + \cos(2\phi)]\Big\}, \tag{28}$$

$$Q_{\rm ey}(t) = \frac{1}{2}\Big\{B_{1\mathcal{N}}(t) + \alpha_1^2 f_1^2(t)(\tanh\alpha_1^2 - 1) + \alpha_2^2|f_2(t)|^2[1 + \cos(2\phi) - 2\exp(-4\alpha_2^2)\sin^2\phi]\Big\}\cdot \tag{29}$$

In these expressions the subscripts ee, oe and ey stand for the initial (signal, idler) modes which are in (ECS, ECS), (OCS, ECS) and (ECS, YSS), respectively. Furthermore, one can note that the significant value of squeezing can be obtained when the pump phase is $\phi = \pm\pi/2$. Also it can be mentioned that the correlation between signal and

idler modes does not occur since cross terms such as $\alpha_1\alpha_2$ are absent. Actually, this is connected with the two-photon nature of ECS and OCS where $\langle \hat{a}_j^m(0)\rangle = 0, j = 1, 2$, when m is an odd integer. It is worth mentioning that the origin of losses caused by reservoirs in expressions (27–29) is the mean photon number. Further, it should be reminded that ECS and YCS can exhibit normal squeezing, which is more pronounced for ECS, however, OCS are unsqueezed states [5].

Further, for the undamped case with $\phi = \pi/2$, expression (28) can be rewritten as

$$Q_{\rm oe}(t) = \frac{1}{2}\Big\{ \sinh^2(gt)[1 + \alpha_2^2(\tanh\alpha_2^2 - 1)] + \alpha_1^2\cosh^2(gt)(\coth\alpha_1^2 - 1)\Big\}\cdot \quad (30)$$

The last term in this expression is non-negative and can become zero by appropriately choosing the value of α_1^2. In order to get squeezing in the signal mode, expression (30) must be negative and this depends on the behaviour of the function $f(x) = x(\tanh x - 1)$. In other words, squeezing can be established if $1 + f(x) < 0$, however, $-0.3 \preceq f(x) < 0$, and consequently squeezing cannot be obtained. More specifically, to obtain single-mode squeezing from this device, the mode under consideration should be prepared initially in a squeezed-cat state regardless of the type of the cat state in the free port (if it is squeezed or not). Furthermore, one can easily estimate how long the single-mode squeezing of the initial light can survive if this light is imposed at the input of the parametric amplifier. Restricting ourselves to the input ECS and using the fact that squeezing is surviving if $Q_{\rm ee}(t) < 0$, the time range over which such a situation occurs is

$$t < \frac{1}{g}\sinh^{-1}\sqrt{\frac{-f(\alpha_1^2)}{1 + f(\alpha_1^2) + f(\alpha_2^2)}}, \quad (31)$$

where $f(x)$ has the same expression as before. For $Q_{\rm oe}(t)$ (*i.e.* Eq. (28)) the procedure shows that the required time is a complex number and this agrees with the previous remark.

From (27) and (29) one can easily verify that the amount of squeezing available in $Q_{\rm ee}(t)$ is much larger than that in $Q_{\rm ey}(t)$ provided that α_2 is finite; nevertheless, when the value of α_2 is zero or large enough, both quantities are typical. This implies that the larger the degree of squeezing in the free port is, the more squeezing will be available in the mode under consideration.

Figure 5 has been displayed to illustrate the behaviour of the Q-squeezing factor for the undamped case when the signal mode is prepared initially in ECS and the idler mode in ECS (solid curve), YSS (short-dashed curve) and OCS (long-dashed curve) in dependence on α_2^2 for the given values of the parameters. Furthermore, the triangle- and star-centred curves represent the underdamped case with a zero-temperature ($\bar{n} = 0$) and a nonzero-temperature heat baths ($\bar{n} \neq 0$), respectively, when the two modes are in ECS. The choice of $\alpha_1^2 = 0.7$ is related to the fact that the initial ECS gives maximum

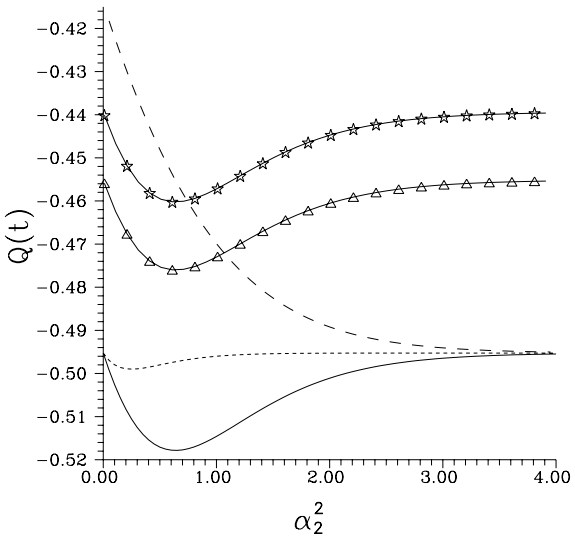

Fig. 5. The single-mode squeezing factor $Q(t)$ for the signal mode being initially in ECS and the idler mode being in ECS (solid curve), YSS (short-dashed curve) and in OCS (long-dashed curve) for $t = 0.2, g = 1, \alpha_1^2 = 0.7, \psi_1 = \psi_2 = 0, \gamma = \bar{n} = 0$ and $\phi = \pi/2$. Triangle- and star-centred curves are given for the squeezing factors of a zero-temperature heat bath ($\bar{n} = 0$) and a nonzero-temperature heat bath ($\bar{n} = 0.1$), respectively, for the underdamped case with $\gamma = 2g - 1.6$ and for the same situation as represented by the solid curve.

squeezing at this value. Now the analytical facts discussed above are remarkable in Figure 5. Further, from this figure we can also see that for the OCS-idler-mode squeezing is minimum when α_2^2 is close to zero (indeed there is a singularity at $\alpha_2 = 0$ related to the nature of the OCS), increasing monotonically as α_2 increases, then it stagnates at large values of α_2 yielding its maximum value. Actually, the behaviour of this case is quite different from the behaviour of the ECS-idler- and YSS-idler-mode cases (compare long-dashed curve with solid and short-dashed curves in Fig. 5), where the maximum value of the former is the minimum value for the latter. This means that for large values of α_2^2 the signal mode can produce the same value of squeezing regardless of the type of the input cat states in the free port. Also this figure shows how one can control the single-mode squeezing relying on the type of initial cat states in the free port.

We now turn our attention to the damped case. As we mentioned earlier $B_{1\mathcal{N}}(t)$ in expressions (27–29) is always positive and therefore the coupling of the system with the environment degrades the amount of the single-mode squeezing. We have given two examples in Figure 5 for the underdamped case (triangle- and star-centred curves). Comparing these curves with the solid one in the same figure, the conclusion becomes clear. Moreover, from the comparison between triangle-centred curve and star-centred curve we can conclude that in nonzero-temperature heat bath case the quantum coherence (*i.e.* nonclassical effects) is lost much faster than in zero-temperature heat bath case [11]. On the other hand, the occurrence of squeezing in the damped case has been

verified also in the behaviour of the W function where for the same values of the parameters we obtained that it always exhibits noise-ellipse forms of cuts together with single-peak or two-peak structure according to α_2 is small or large, respectively. It is worth mentioning that for the cat states interacting with heat bath the authors of [5] claimed that squeezing is much more robust with respect to damping than the oscillations in the photon-number distribution or the interference in phase space described by W function. They obtained this conclusion by analyzing these quantities graphically. Nevertheless, in their analysis, squeezing has been obtained for a specific region of α (in particular when α is small) whereas the behaviour of the photon-number distribution and the W function has been analyzed in a different region (when $\alpha = 2$, where squeezing does not occur, see Fig. 8a in [5]). This leads to the incorrect conclusion. We have examined the behaviour of both the photon-number distribution and the W function for these cases using the same values of the parameters as in [5], however, we have taken $\alpha = 1$ (where squeezing is noticeable) and found that the behaviour of these quantities reflects equally the properties of squeezed light. For more details reader can consult [42].

Finally, for the single-mode reduced factorial moments, which can be measured by a set of photodetectors, we have found that the behaviour of these quantities is in a good agreement with the behaviour of the single-mode squeezing.

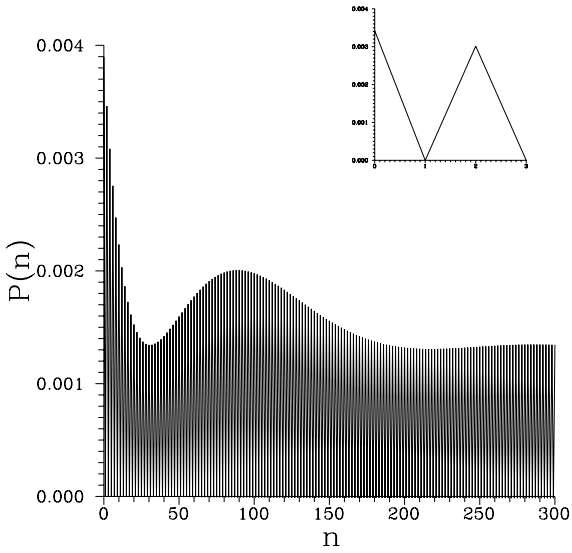

Fig. 6. Sum photon-number distribution when the signal and idler modes are prepared initially in ECS with $|\alpha_1| = 3, |\alpha_2| = 2, g = 10^4, t = 3 \times 10^{-4}, \psi = \pi/2$. On the right corner of the figure the scheme shows the parity of the photon-number sum.

4 Results for the compound-mode case

In this section we demonstrate the two-mode properties for the system under discussion by determining the sum photon-number distribution, two-mode squeezing and reduced factorial moments.

4.1 Sum photon-number distribution

The oscillations in the joint photon-number distribution might be observed in experiments that generate two-mode squeezed light in which the two modes may be distinguished by frequency or by propagation direction. Having separated the two modes, as was done by using a polarizing beamsplitter [43], one can send them directly onto separate photocounters and then build up the joint photon-number distribution from the photocount statistics of a sequence of pulses [44].

It has been shown [27] that the sum photon-number distribution $P(n)$ of the nondegenerate parametric amplifier, when the modes are initially prepared in coherent state and under certain conditions, displays two regimes, which exhibit either single-peak structure or oscillatory behaviour. The single-peak structure can be narrower (or broader) than that of the corresponding Poissonian distribution showing nonclassical (or classical) effects. The striking feature is that the $P(n)$ can exhibit, for certain choice of the interaction parameters, collapses and revivals in the photon-number domain somewhat similar to those known in the JCM. For the present system the situation is rather complicated regarding to the evolution of the density matrix (8) where the interference in phase space is established. Excluding dissipation and using $\psi = \pm\pi/2$ as in [27], we have seen generally that $P(n)$ exhibits always oscillatory behaviour irrespective of which type of cat states has been considered initially. Moreover, $P(n)$ can yield pairwise oscillations identifying that even or odd photons are being observed. Figures 6 and 7 have been plotted to show such a phenomenon for given values of the parameters. From Figure 6 we observe that the long scale oscillations in the behaviour of $P(n)$ with $P(2n + 1) = 0$ are somewhat similar to those of squeezed states [45]. Actually for squeezed states the pairwise oscillations are explained as a direct consequence of the quadratic, or two-photon nature of the squeeze operator $\hat{S}(r)$, *i.e.* $\hat{S}(r) = \exp[r(\hat{a}^2 - \hat{a}^{\dagger 2})/2]$ [45]. However, here the origin of the pairwise oscillations in $P(n)$ is in the competition between the processes described by three parts of the density matrix of the field. Figures 7a–7c give insight into this point, *i.e.* they show the manner in which the photon-number distributions of the three parts of the density matrix (8) compete. More precisely, Figures 7a, 7b and 7c represent the sum photon-number distributions $P_{\rm M}(n), P_{\rm SI}(n)$ and $P_{\rm AI}(n)$ associated with $\hat{\rho}_{\rm M}(0), \hat{\rho}_{\rm SI}(0)$ and $\hat{\rho}_{\rm AI}(0)$, correspondingly. Figure 7a shows revival-collapse pattern, which is resulting from the statistical mixture part (9). Furthermore, from this figure one can observe that when the number of photons increases, the amplitude of the revivals diminishes, but the revival periods extend. It is worth mentioning that such a quantum collapse-revival phenomenon has been seen

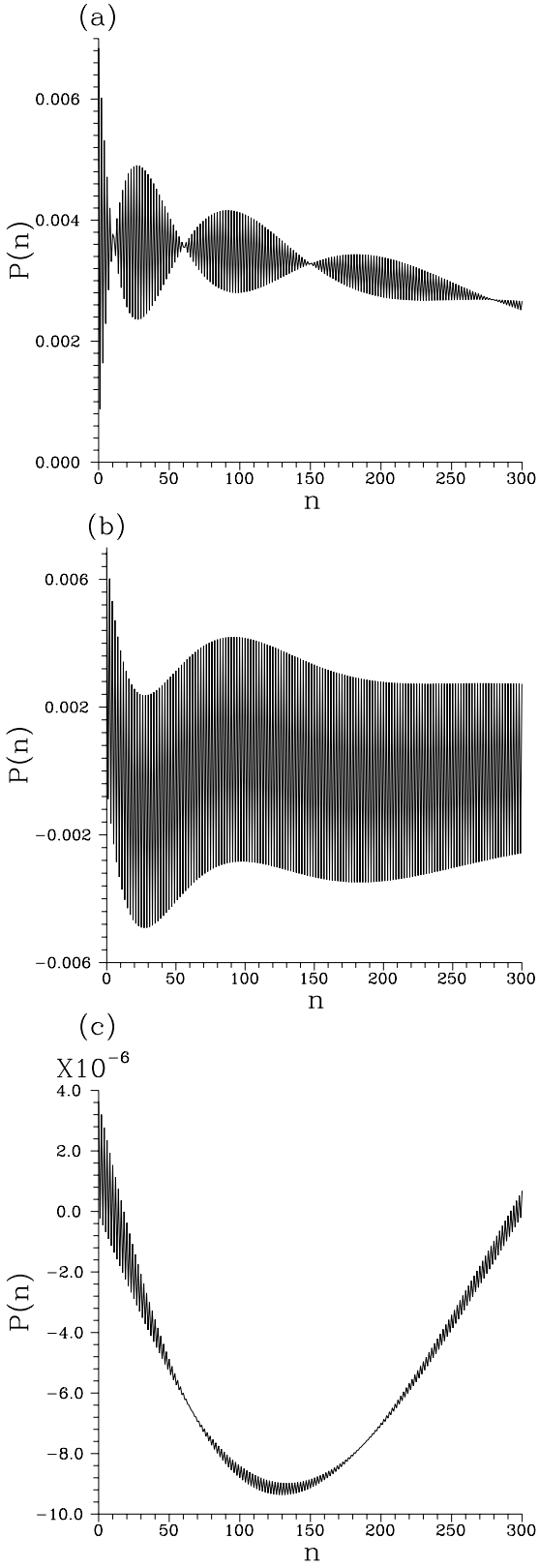

Fig. 7. Sum photon-number distributions corresponding to the three parts of the density matrix for the same values of the parameters as in Figure 6 and for: (a) $P(n)$ resulting from $\hat{\rho}_{\rm M}(0)$; (b) $P(n)$ resulting from $\hat{\rho}_{\rm SI}(0)$; and (c) $P(n)$ resulting from $\hat{\rho}_{\rm AI}(0)$.

for the photon-number distribution of single-mode [46] and two-mode [47] squeezed coherent states with complex squeeze and displacement parameters. Associations with the quantum phases of the modes may be considered [47,48], (also [34] p. 281). From Figure 7b it is clear that $P_{\rm SI}(n)$ oscillates between negative and positive values. Comparison of Figures 7a, 7b and 7c shows that the values of $P_{\rm AI}(n)$ are approximately negligible compared with those of $P_{\rm M}(n)$ and $P_{\rm SI}(n)$. Now if we turn our attention back to Figure 6 we can recognize that the competition between $P_{\rm M}(n)$ and $P_{\rm SI}(n)$ leads to the destruction of collapse-revival phenomenon (which appeared in Fig. 7a), however, the distribution "evolves" in an interesting manner similarly as that for squeezed states. In fact, the situation here is in contrast with that of the evolution of cat states in the JCM where the interference in phase space makes the revival-collapse phenomenon in the atomic inversion more pronounced when the revival time equals the half of that for the standard JCM with initial coherent light [17]. The reason is that for the latter case the distribution of the spectral components of the atomic inversion is one-dimensional distribution since only one mode is involved, whereas here we have two-dimensional superimposed distributions. Further, we have obtained that the oscillations in $P(n)$ increase if either g or t or both are increased. This fact is clear if we look at the problem as evolution of cat states under the action of two-mode squeeze operator, where the squeezing parameter in this case is $r = gt$ and the oscillations become more pronounced for the large values of r [44,49]. In conclusion, for the system under consideration the origin of the oscillations in the sum photon-number distribution is two-fold:

(i) the interference in phase space;
(ii) the strong coupling between the signal and idler modes of the system in the course of the interaction time.

On the other hand, we have found by an explicit algebraic calculation for all quantities studied in this paper excepting quadrature squeezing that the contributions associated with elements of $\hat{\rho}_{\rm SI}(0)$ and $\hat{\rho}_{\rm AI}(0)$ involve $\cos(\phi_1 \pm \phi_2)$ and $\cos\phi_{1,2}$, respectively. This fact together with the information included in Figures 7 show that $P(n)$ can collapse and yield decoherence in relation to distribution for statistical mixture part using specific types of cat states initially. More illustratively, preparing one of the modes initially in ECS (or OCS) and the other in YSS or *vice versa*, the $P(n)$ evolves as described by Figure 7a (for the same values of the parameters). This shows how one can decohere the system apart from the amplification nature of the system and without coupling it to the environment. We call such a type of decoherence a phase decoherence. Actually, for some quantities the contribution of off-diagonal elements of the density matrix is responsible for the nonclassical effects, *e.g.* as we will see below in the compound-mode reduced factorial moments. Then we can make a good estimation of these phenomena using such a property. The final remark is that the nonclassical effects for the compound-mode case are much

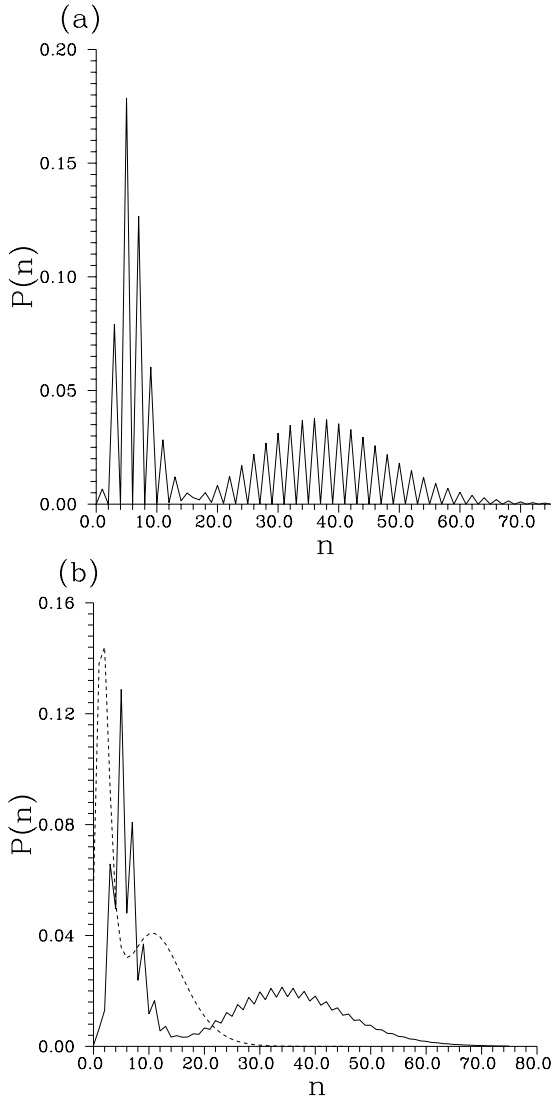

Fig. 8. Sum photon-number distribution for (a) undamped case with the values of the parameters as those of the solid curve in Figure 3; (b) damped case with $(g, \bar{n}, \gamma) = (0.5, 0.5, 2g - 0.9)$ (underdamped case-solid curve) and $(0.5, 0.5, 2g + 0.1)$ (overdamped case-dashed curve).

richer than those for the single-mode case. This results from the strong quantum correlation between the signal and idler modes, which manifests itself as the summation in expressions (19) and (20). To make this point clear, we give Figure 8a for the $P(n)$ and for the same situation as that of the solid curve in Figure 3. The comparison between these two figures is instructive. Further, Figure 8b includes information on the damped case where one can observe smooth oscillations for the underdamped case (solid curve) and two-peak structure for the overdamped case (dashed curve). Specifically, for the overdamped case the off-diagonal elements are completely suppressed.

4.2 Two-mode squeezing and reduced factorial moments

Firstly, we will discuss two-mode squeezing, which can be measured by heterodyne detection where squeezing is carried jointly by two modes of different frequencies and the local oscillator has a frequency midway in between [50]. We proceed taking into account that the nondegenerate parametric amplifier is well described by the two-mode squeeze operator. Actually, two-mode squeezing phenomenon is essentially connected with the states upon which such operator acts. In other words, squeezing may not exist for some specific states even if they include two-mode squeeze operator in their structures. To show this we give the form of the two-mode squeezing factor Q when the signal and idler modes are initially prepared in cat states, excluding losses, considering $\alpha_j, j = 1, 2$, are real and $\phi = 0$. In this case the squeezing factor Q takes the form

$$Q(t) = \frac{1}{2}[Q_1(t) + Q_2(t)], \tag{32}$$

where $Q_j(t), j = 1, 2$, represent the corresponding single-mode squeezing factors of the signal and idler modes, respectively. From expression (32) it is clear that the correlation between the signal and idler modes does not exist since $\langle \hat{Y}_1 \hat{Y}_2 \rangle = \langle \hat{Y}_1 \rangle \langle \hat{Y}_2 \rangle$, where $\langle \hat{Y}_j \rangle, j = 1, 2$, are the expectation values of the Y-quadrature of the signal and idler modes. The existence of correlation between these two modes is important to obtain squeezing in the compound modes even if the individual modes are not themselves squeezed [49]. Expression (32) shows that interference in phase space can destroy squeezing and also that the rates of degradation of the two-mode and single-mode squeezing are on the same level for symmetrical losses. Also it is obvious that the two-mode squeezing can be realized if at least one of the two modes (signal or idler) can exhibit single-mode squeezing. This is necessary but not sufficient condition. Further, the maximum squeezing may be produced when both the signal and idler modes exhibit maximum single-mode squeezing. This reflects the importance of the choice of the type of the initial cat states. From the discussion in Section 3 it is obvious that when the two modes are initially in OCS, the interaction cannot generate two-mode squeezing.

We now discuss the case that one of the modes is initially squeezed (ECS) and the other is unsqueezed (OCS) for the same situation as that in (32). The required time to obtain squeezing in the compound-mode case ($Q(t) < 0$) is

$$\sinh(gt) < \sqrt{\frac{-|\alpha_1|^2(\tanh|\alpha_1|^2 - 1) - |\alpha_2|^2(\coth|\alpha_2|^2 - 1)}{2(1 + |\alpha_1|^2 \tanh|\alpha_1|^2 + |\alpha_2|^2 \coth|\alpha_2|^2)}}\,. \tag{33}$$

This inequality gives relation between the squeeze time and the "distances" between the states, which are forming the cats. So that the length of the device can be adjusted to obtain squeezed light. An analysis to the right-hand

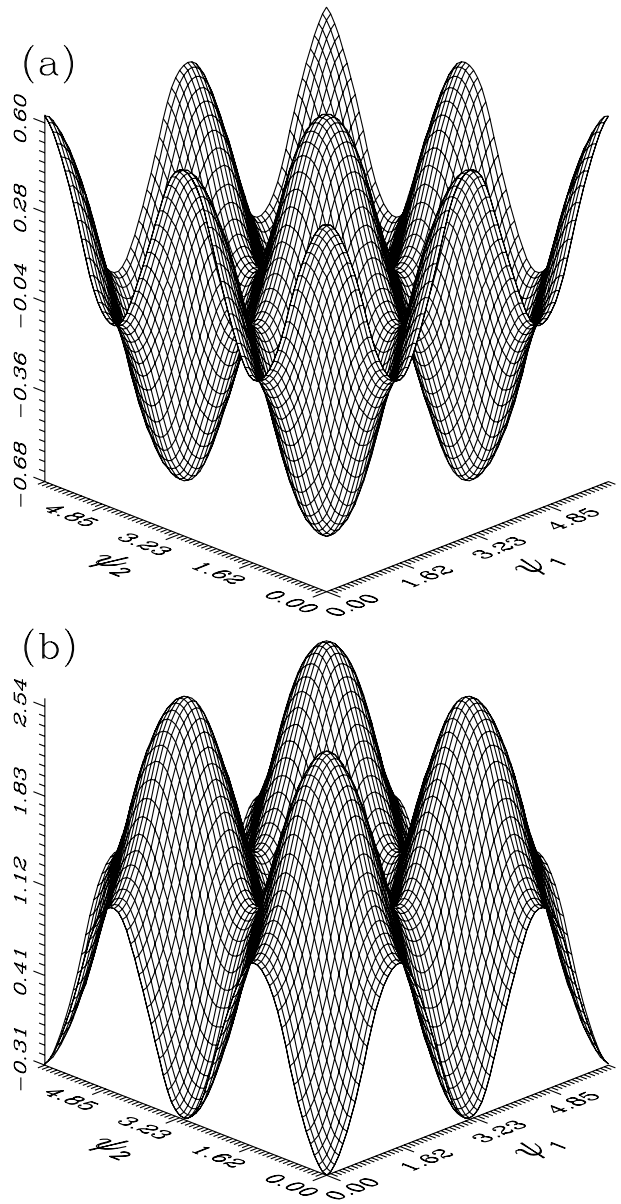

Fig. 9. The compound two-mode squeezing against $\psi_j, j = 1, 2$, for undamped case when the signal and idler modes are initially prepared in ECS for $t = 0.2, |\alpha_j| = 0.7, g = 1, \phi = \pi/2$: (a) squeezing factor S; (b) squeezing factor Q.

side of (33) gives that the maximum scaled time (effective time) for squeezing is $\tau = gt \simeq 0.1769$ at $(|\alpha_1|, |\alpha_2|) = (0.6, 2.4)$. It is worth mentioning at this point that the Y-component quadrature squeezing of ECS takes on its maximum, whereas that of OCS vanishes.

On the other hand, when the phase information is included (*i.e.* $\psi_j \neq 0, \phi \neq 0$) the situation is improved in such a way that squeezing can be detected in both quadratures provided that one of the modes is initially prepared in a squeezed-cat state, *i.e.* in ECS or YSS. The role of the phase is analyzed in Figures 9a and 9b where we have plotted the squeezing factors corresponding to X-component and Y-component, respectively, when the signal and idler modes are initially prepared in ECS. From these figures we can see that maximum squeezing occurs in X-component and locates at $(\psi_1, \psi_2) = (m_1\pi, m_2\pi), m_j = 1/2, 3/2$. The opposite situation can be observed for the Y-component where squeezing also exists but it is less pronounced and locates at $(\psi_1, \psi_2) = (m_1\pi, m_2\pi), m_j = 0, 1, 2$, *i.e.* the extreme values are exchanged. Such a behaviour in the two quadratures indicates that the uncertainty relation holds. Further, for $\phi = -\pi/2$ we obtained similar behaviour, however, the maximum squeezing values would be available in the Y-component. Further similar behaviour can be seen if the other types of cat states are used. It is remarkable that the behaviour of squeezing in the present interaction is quite different from that for both ECS [3] and two-mode squeezed coherent states [49] where for both squeezing exists only in one of the two quadrature components; perfect squeezing (*i.e.* 100% squeezing) occurs only for the two-mode squeezed coherent states. In conclusion the squeezing phenomenon discussed here is a manifestation of co-operative effects among the phases of the different components of the system. Furthermore, by controlling the phases in this device, squeezing can be amplified and switched between the two quadratures.

We would like to conclude this subsection by shedding the light on the behaviour of the reduced factorial moments for the compound-mode case. In this case the antibunched light can be measured if both the signal and idler modes are simultaneously detected by means of two photodetectors and then their outputs are correlated. Generally, reduced factorial moments can evolve to produce nonclassical negative values based on the types of initial cat states. Further, we have checked that the contribution of $\hat{\rho}_{\rm M}(0)$ cannot produce antibunched light independently. These two facts reflect the role of the phase decoherence property discussed above. On the other hand, similar argument as that for the single-mode case can be given here except the case when the two modes are in YSS where a slight antibunching can be observed, but only for certain values of the interaction parameters. Figure 10 shows the reduced factorial moments of the compound-mode case for the given values of the parameters. In this figure we have used the normalized factor $K_c\,(= \langle W^k\rangle/\langle W\rangle^k - 1)$, where the nonclassical effect occurs when $K_c < 0$. From this figure, it is interesting to observe that the behaviour of the reduced factorial moments when the (signal, idler) modes are in (OCS, OCS) is very close to the behaviour of the second-order correlation function of OCS [5] provided that $|\alpha_j|, j = 1, 2$, are finite.

5 Conclusions

In this paper we have analyzed the properties of the dissipative parametric amplifier when the signal and idler modes are initially prepared in Schrödinger-cat states. Needless to say the present interaction as described by the Hamiltonian (3) and the density matrix (8) is much more complicated than that in the simple case of a harmonic oscillator coupled with the heat bath [11–18]. After

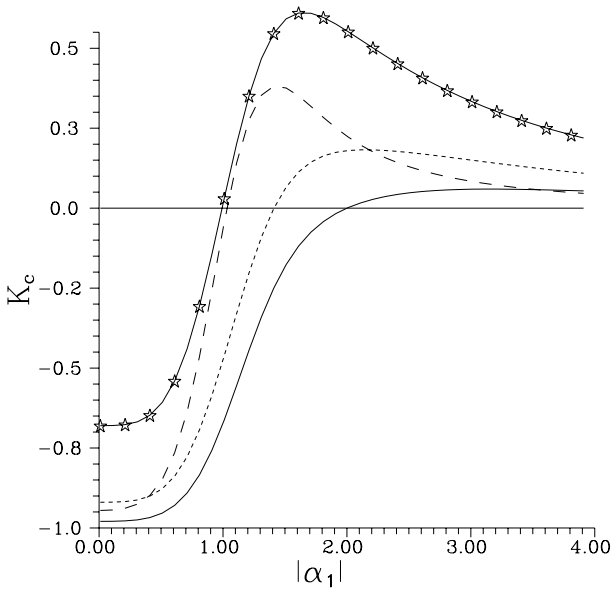

Fig. 10. The compound-mode reduced factorial moments ($K_c = \langle W^k\rangle/\langle W\rangle^k - 1$) against $|\alpha_1|$ for $k = 5, \psi = \pi/2, t = 0.2, |\alpha_2| = 0.25, g = 0.5$, and for the undamped case when the signal and idler modes are prepared initially in (OCS, OCS) (solid curve) and (OCS, ECS) (long-dashed curve). The damped case is considered for the same situation as the solid curve, but for the underdamped case (short-dashed curve) $(\gamma, \bar{n}) = (2g - 0.6, 0.5)$ for the overdamped case (star-centred curve) $(\gamma, \bar{n}) = (2g + 0.1, 0.5)$. The straightline shows the antibunching bound.

obtaining the solution of the Heisenberg–Langevin equations quantum statistics of interacting modes have been investigated based on the normally ordered characteristic functions. The system of damping oscillators has been assumed to have a flat spectrum and a chaotic distribution.

In general, there are two operations controlling the behaviour of the interaction which are the interference in phase space and the entanglement. Intuitively, the initial macroscopic cat states cannot be preserved in the system. Furthermore, for long-time interaction the initial nonclassical effects of the cats are degraded by the amplification dynamics inherent in the system and the cumulative effects of dissipation. Excluding dissipation we have shown that if the input to the device are squeezed (sub-Poissonian) cat states, then the output may be squeezed (antibunched) too provided that the interaction time and gain are finite. Furthermore, the device could be used to amplify squeezing in the compound-mode case. On the contrary, the well-known role of the parametric amplifier as a source of perfect squeezing in the compound-mode case rather than in single-mode case fades out for input cat states. The photon-number distribution can exhibit oscillatory behaviour, which is more pronounced in the compound-mode case than in the single-mode case, regardless of the types of the initial cat states. Also we have shown that the decoherence can arise in the system from the decay of the pump and the phase control.

For dissipation case we have considered in detail only two cases which are related to underdamped and overdamped regimes. In these cases the interaction tends to eliminate the off-diagonal elements of the density matrix and to affect the diagonal elements. It has been found that the dynamical subsystems (signal or idler modes) collapse to the statistical mixture state or thermal state according to whether the underdamped regime or overdamping regime is considered. Further, we have also shown that the single-mode squeezing at nonzero temperature of the environment decreases much faster than that at zero temperature, however, this situation is generally valid for all quantities studied in this paper. In conclusion, the losses uniformly distributed over the device deteriorate its operational characteristics. Of course, such deterioration is more pronounced for the overdamped case. Finally, the inclusion of lossy mechanics in the system is of a great interest for accurate measurements.

J.P., V.P. and F.A.A.E.-O. acknowledge the partial support from the Project LN00A015 of the Czech Ministry of Education. One of us (M.S.A.) is grateful for the financial support from the Project Math 1418/19 of the Research Centre, College of Science, King Saud University.

Appendix A

In this appendix we give the explicit forms for the time-dependent coefficients $(f_j(t), \Gamma_{jl}(t), \Gamma'_{jl}(t))$ of the solution of the Heisenberg–Langevin equations of the Hamiltonian (3) (for details see [30,31]):

$$f_1(t) = \frac{1}{\sqrt{\epsilon}} \exp\left[-\frac{(\gamma_1+\gamma_2)t}{4}\right]\left[\sqrt{\epsilon}\cosh\left(\frac{\sqrt{\epsilon}}{4}t\right) + (\gamma_2-\gamma_1)\sinh\left(\frac{\sqrt{\epsilon}}{4}t\right)\right], \tag{A.1}$$

$$f_2(t) = \frac{4\mathrm{i}g\exp(\mathrm{i}\phi)}{\sqrt{\epsilon}} \exp\left[-\frac{(\gamma_1+\gamma_2)t}{4}\right]\sinh\left(\frac{\sqrt{\epsilon}}{4}t\right), \tag{A.2}$$

$$f_3(t) = \frac{1}{\sqrt{\epsilon}} \exp\left[-\frac{(\gamma_1+\gamma_2)t}{4}\right]\left[\sqrt{\epsilon}\cosh\left(\frac{\sqrt{\epsilon}}{4}t\right) + (\gamma_1-\gamma_2)\sinh\left(\frac{\sqrt{\epsilon}}{4}t\right)\right], \tag{A.3}$$

$$\begin{aligned}\Gamma_{jl}(t) = {} & \frac{-\mathrm{i}k_{jl}}{\epsilon'^2_{jl} - \frac{\epsilon}{16}} \exp\left[-\frac{(\gamma_1+\gamma_2)t}{4}\right] \\ & \times \left\{\sqrt{\epsilon}\left[\epsilon'_{jl} + (-1)^{j+1}\frac{(\gamma_2-\gamma_1)}{4}\right]\right. \\ & \times \left[\exp(\epsilon'_{jl}t) - \cosh\left(\frac{\sqrt{\epsilon}}{4}t\right)\right] \\ & \left. - \left[\frac{\epsilon}{4} + (-1)^{j+1}(\gamma_2-\gamma_1)\epsilon'_{jl}\right]\sinh\left(\frac{\sqrt{\epsilon}}{4}t\right)\right\}, \\ & j = 1, 2,\end{aligned} \tag{A.4}$$

$$\Gamma'_{jl}(t) = \frac{-2\mathrm{i}g\exp(\mathrm{i}\phi)k_{jl}}{\epsilon'^2_{jl} - \frac{\epsilon}{16}} \exp\left[-\frac{(\gamma_1+\gamma_2)t}{4}\right] \times \left\{ \frac{\sqrt{\epsilon}}{2}\left[\exp(\epsilon'_{jl}t) - \cosh\left(\frac{\sqrt{\epsilon}}{4}t\right)\right] - 2\epsilon'_{jl}\sinh\left(\frac{\sqrt{\epsilon}}{4}t\right)\right\}, \quad j=1,2, \tag{A.5}$$

where

$$\epsilon = (\gamma_1-\gamma_2)^2 + 16g^2, \quad \epsilon'_{jl} = \frac{1}{4}(\gamma_1+\gamma_2) + \mathrm{i}(\omega_j - \varphi_{jl}). \tag{A.6}$$

Appendix B

In this appendix we write down the explicit forms for the quantities $(B_{j\mathcal{N}}(t), D(t))$ in the expression (13) (for details see [30,31]):

$$B_{1\mathcal{N}}(t) = B_{1\mathcal{N}}(\gamma_1,\gamma_2,\langle n_{1d}\rangle,\langle n_{2d}\rangle,t) = \frac{1}{\epsilon}\Big\{8g^2E_1 + \frac{\gamma_1\langle n_{1d}\rangle}{\gamma_1\gamma_2-4g^2}\Big[\left(\gamma_2\epsilon - 4g^2(\gamma_1+\gamma_2)\right)E - \sqrt{\epsilon}\left(\gamma_2(\gamma_2-\gamma_1)+4g^2\right)F\Big] + \frac{4\gamma_2g^2(1+\langle n_{2d}\rangle)}{\gamma_1\gamma_2-4g^2}[(\gamma_1+\gamma_2)E - \sqrt{\epsilon}F] - 16g^2G[\gamma_2(1+\langle n_{2d}\rangle) - \gamma_1\langle n_{1d}\rangle]\Big\} \tag{B.1}$$

$$B_{2\mathcal{N}}(t) = B_{1\mathcal{N}}(\gamma_2,\gamma_1,\langle n_{2d}\rangle,\langle n_{1d}\rangle,t), \tag{B.2}$$

$$D(t) = \frac{2g\exp(-\mathrm{i}\phi)}{\epsilon}\Big\{(\gamma_2-\gamma_1)E_1 - \sqrt{\epsilon}F + \frac{\gamma_1\langle n_{1d}\rangle}{\gamma_1\gamma_2-4g^2}[(\gamma_1\gamma_2-\gamma_2^2-8g^2)E + \gamma_2\sqrt{\epsilon}F] + \frac{\gamma_2(1+\langle n_{2d}\rangle)}{\gamma_1\gamma_2-4g^2}[(\gamma_1\gamma_2-\gamma_1^2-8g^2)E + \gamma_1\sqrt{\epsilon}F] + 2G[\gamma_1\langle n_{1d}\rangle(\gamma_2-\gamma_1) + \gamma_2(1+\langle n_{2d}\rangle)(\gamma_1-\gamma_2)]\Big\}, \tag{B.3}$$

$$\begin{aligned}\bar{\alpha}_1(t) &= \alpha_1^* f_1(t) + \alpha'_2 f_2^*(t),\\ \bar{\alpha}_2(t) &= \alpha'_1 f_2^*(t) + \alpha_2^* f_3(t),\\ \bar{\alpha}'_1(t) &= \alpha'_1 f_1(t) + \alpha_2^* f_2(t),\\ \bar{\alpha}'_2(t) &= \alpha_1^* f_2(t) + \alpha'_2 f_3(t),\end{aligned} \tag{B.4}$$

while

$$E = 1 - \exp\left[-\frac{(\gamma_1+\gamma_2)t}{2}\right]\cosh\left(\frac{\sqrt{\epsilon}}{2}t\right), \tag{B.5a}$$

$$E_1 = \exp\left[-\frac{(\gamma_1+\gamma_2)t}{2}\right]\left[\cosh\left(\frac{\sqrt{\epsilon}}{2}t\right) - 1\right], \tag{B.5b}$$

$$F = \exp\left[-\frac{(\gamma_1+\gamma_2)t}{2}\right]\sinh\left(\frac{\sqrt{\epsilon}}{2}t\right), \tag{B.5c}$$

$$G = \frac{1}{\gamma_1+\gamma_2}\left\{1 - \exp\left[-\frac{(\gamma_1+\gamma_2)t}{2}\right]\right\}. \tag{B.5d}$$

A generalization to the case when the total density operator is not factorized and the correlation between the system and reservoirs is present, may be excluded [51].

References

1. E. Schrödinger, Nature **23**, 844 (1935)
2. B. Yurke, D. Stoler, Phys. Rev. Lett. **57**, 13 (1986); M. Hillery, Phys. Rev. A **36**, 3796 (1986); Y. Xia, G. Guo Phys. Lett. A **136**, 281 (1989); C.C. Gerry, Opt. Commun. **91**, 47 (1992); J. Janszky, A.V. Vinogradov, Phys. Rev. Lett. **64**, 2771 (1990); J. Sun, J. Wang, C. Wang, Phys. Rev. A **46**, 1700 (1992).
3. W. Schleich, M. Pernigo, F. Le Kien, Phys. Rev. A **44**, 2172 (1991)
4. M. Brune, S. Haroche, J.M. Raimond, L. Davidovich, N. Zagury, Phys. Rev. A **45**, 5193 (1992)
5. V. Bužek, A. Vidiella-Barranco, P.L. Knight, Phys. Rev. A **45**, 6570 (1992)
6. J. Milburn, C.A. Holmes, Phys. Rev. A **56**, 2237 (1986); J. Milburn, Phys. Rev. A **33**, 674 (1986); A. Mecozzi, P. Tombesi, Phys. Rev. Lett. **58**, 1055 (1987); P. Tombesi, A. Mecozzi, J. Opt. Soc. Am. B **4**, 1700 (1987); M. Wolinsky, H.J. Carmichael, Phys. Rev. Lett. **60**, 1836 (1988); B.C. Sanders, Phys. Rev. A **39**, 4284 (1989); C.M. Savage, W.A. Cheng, Opt. Commun. **70**, 439 (1989); A. Miranowicz, R. Tanaś, S. Kielich, Quant. Opt. **2**, 253 (1990)
7. A. La Porta, R.E. Slusher, B. Yurke, Phys. Rev. Lett. **62**, 26 (1989); S. Song, C.M. Caves, B. Yurke, Phys. Rev. A **41**, 5261 (1990); B. Yurke, J. Opt. Soc. Am. B **3**, 732 (1986); B. Yurke, W. Schleich, D.F. Walls, Phys. Rev. A **42**, 1703 (1990)
8. J.J. Slosser, P. Meystre, E.M. Wright, Opt. Lett. **15**, 223 (1990); J.J. Slosser, P. Meystre, Phys. Rev. A **41**, 3867 (1990); M. Wilkens, P. Meystre, Phys. Rev. A **43**, 3832 (1991)
9. S. Schaufler, M. Freyberger, W.P. Schleich, J. Mod. Opt. **41**, 1765 (1994)
10. S.-B. Zheng, G.-C. Guo, Opt. Commun. **138**, 317 (1997)
11. M.S. Kim, V. Bužek, Phys. Rev. A **46**, 4239 (1992)
12. M.S. Kim, V. Bužek V, Phys. Rev. A **47**, 610 (1993)
13. M.S. Kim, K.S. Lee, V. Bužek, Phys. Rev. A **47**, 4302 (1993)
14. V. Bužek, M.S. Kim, Ts. Gantsog, Phys. Rev. A **48**, 3394 (1993)
15. U. Leonhardt, Phys. Rev. A **48**, 3265 (1993)
16. P. Domokos, J. Janszky, Phys. Lett. A, **186** 289 (1994)
17. A. Vidiella-Barranco, H. Moya-Cessa, V. Bužek, J. Mod. Opt. **39** 1441 (1992)
18. R. Filip, J. Opt. B: Quant. Semiclass. Opt. **3**, S1 (2001)
19. L. Diósi, N. Gisin, W.T. Strunz, Phys. Rev. A **58**, 1699 (1998)
20. S.K. Zhang, M. Fujita, M. Yamanaka, M. Nakatsuka, Y. Izawa, C. Yamanaka, Opt. Commun. **184**, 451 (2000)

21. P.G. Kwiat, W.A. Vareka, C.K. Hong, H. Nathel, R.Y. Chiao, Phys. Rev. A **41**, 2910 (1990); Z.Y. Ou, X.Y. Zou, L.J. Wang, L. Mandel, Phys. Rev. Lett. **65**, 321 (1990)
22. X.Y. Zou, L.J. Wang, L. Mandel, Phys. Rev. Lett. **67**, 318 (1991)
23. L. Mišta, J. Peřina, Czech J. Phys. B **28**, 392 (1978)
24. B.R. Mollow, R.J. Glauber, Phys. Rev. **160**, 1076; *ibid.* 1097 (1967)
25. L. Mišta, Czech J. Phys. B **19**, 443 (1969)
26. L. Mišta, J. Peřina, Acta Phys. Pol. A **52(3)**, 425 (1977)
27. F.A.A. El-Orany, J. Peřina, M.S. Abdalla, Opt. Commun. **187**, 199 (2001)
28. E.T. Jaynes, F. Cummings, Proc. IEEE **51**, 89 (1963); N.H. Eberly, N.B. Norozhny, J.J. Sanchez-Mondragon, Phys. Rev. Lett. **44**, 1323 (1980)
29. S.J.D. Phoenix, P.L. Knight, Ann. Phys. **186**, 381 (1988)
30. V. Peřinová, Opt. Act. **28**, 747 (1981)
31. V. Peřinová, J. Peřina, Opt. Act. **28**, 769 (1981)
32. J. Peřina, *Quantum Statistics of Linear and Nonlinear Optical Phenomena*, 2nd edn. (Kluwer, Dordrecht, 1991)
33. L. Mandel, E. Wolf, *Optical Coherence and Quantum Optics* (Univ. Press, Cambridge, 1995)
34. V. Peřinová, A. Lukš, J. Peřina, *Phase in Optics* (World Scientific, Singapore, 1998)
35. D.T. Smithey, M. Beck, J. Cooper, M.G. Raymer, Phys. Rev. A **48**, 3159 (1993); M. Beck, D.T. Smithey, M.G. Raymer, Phys. Rev. A **48**, 890 (1993); M. Beck, D.T. Smithey, J. Cooper, M.G. Raymer, Opt. Lett. **18**, 1259 (1993); D.T. Smithey, M. Beck, J. Cooper, M.G. Raymer, M.B.A. Faridani, Phys. Scr. T **48**, 35 (1993)
36. G.S. Agarwal, Phys. Rev. A **59**, 3071 (1999)
37. D. Mogilevtsev, S.Y. Kilin, Opt. Commun. **132**, 452 (1996)
38. A. Bandilla, H-H. Ritze, Opt. Commun. **34**, 190 (1980)
39. R. Bonifacio, S. Olivares, P. Tombesi, D. Vitali, J. Mod. Opt. **47**, 2199 (2000)
40. S.L. Braunstein, H.J. Kimble, Phys. Rev. Lett. **80**, 869 (1998); G.J. Milburn, S.L. Braunstein, Phys. Rev. A **60**, 937 (1999); T.C. Ralph, Phys. Rev. A **61**, 010303(R) (2000); M. Hillery, Phys. Rev. A **61**, 022309 (2000)
41. F.A. Popp, J.J. Chang, A. Herzog, Z. Yan, Y. Yan, Phys. Lett. A **293**, 98 (2002)
42. F.A.A. El-Orany, Phys. Rev. A **65**, 043814 (2002)
43. O. Aytür, P. Kumar, Phys. Rev. Lett. **65**, 1551 (1990)
44. C.C. Caves, C. Zhu, G.J. Milburn, W. Schleich, Phys. Rev. A **43**, 3854 (1991)
45. H.P. Yuen, Phys. Rev. A **13**, 2226 (1976)
46. B. Dutta, N. Mukunda, R. Simon, A. Subramaniam, J. Opt. Soc. B **10**, 253 (1993)
47. M. Selvadoray, M.S. Kumar, R. Simon, Phys. Rev. A **49**, 4957 (1994)
48. M. Selvadoray, M.S. Kumar, Opt. Commun. **136**, 125 (1997)
49. S.M. Barnett, P.L. Knight, J. Mod. Opt. **34**, 841 (1987)
50. R. Loudon, P.L. Knight, J. Mod. Opt. **34**, 709 (1987)
51. C.W. Gardiner, M.J. Collett, Phys. Rev. A **31**, 3761 (1985)